Computers in Biology and Medicine 180 (2024) 108976

Contents lists available at ScienceDirect

Computers in Biology and Medicine

journal homepage: www.elsevier.com/locate/compbiomed

Modeling biological growth of human keratoconus: On the effect of tissue degradation, location and size

Benedetta Fantaci [a,*], Begoña Calvo [a,b], José Félix Rodríguez [c]

[a] Aragon Institute of Research Engineering (I3A), Universidad de Zaragoza, Zaragoza, Spain
[b] Bioengineering, Biomaterials and Nanomedicine Networking Biomedical Research Centre (CIBER-BBN), Universidad de Zaragoza, Zaragoza, Spain
[c] LaBS, Department of Chemistry, Materials and Chemical Engineering "Giulio Natta", Politecnico di Milano, Milan, Italy

ARTICLE INFO

Keywords:
Keratoconus
Growth formulation
Tissue degradation
Finite element modeling
Cornea
Continuum solid mechanics

ABSTRACT

Keratoconus is a non-inflammatory bilateral disease, that usually occurs in the inferior-temporal region, where the cornea bulges out and becomes thinner, due to the gradual loss of structural organization in corneal tissue. Degenerated extracellular matrix and fibers breakage have been observed in keratoconic corneas, that may promote the progression of the pathology. While keratoconus histopathology has been widely described in literature, its etiology is still not clear. Being able to fully understand keratoconus growing process could be crucial to detect its development and improve prevention strategies. This work proposes a novel continuum-based keratoconus growth model. The proposed framework accounts for the structural changes occurring in the underlying tissue during the progression of the disease, as indicated in experiments. The developed formulation is able to replicate the typical bulging and thinning of keratoconic corneas, as well as different forms in terms of shape, as they are commonly classified in clinics (nipple, oval and globus cones). The cone that is obtained constitutes a permanent deformed state, not pressure dependent. The resulting model may help to better understand the etiology of the behavior of this disease with the aim of improving the diagnosis and the treatment of the pathology.

1. Introduction

Cornea is the primary refractive surface and dictates the quality of our vision thanks to its high transparency and curved shape [1]. Being both a lens and a biological structure, it behaves as a biomechanical support to balance the effect of the intraocular pressure (IOP), generated by the humors inside the eyeball cavity. Corneal structure is made of five different layers (epithelium, Bowman's layer, stroma, Descemet's membrane and endothelium), among which the stroma constitutes the 90% and is mostly responsible for the tissue biomechanical response. The high transparency needed to act as a lens is provided by the precise organization of the collagen fibers in the stroma, embedded in the extracellular matrix (ECM). Collagen fibers are organized in fibrils, which in turn are packed in lamellae. The lamellae show a preferred orientation in the nasal-temporal and inferior–superior directions in the posterior third of the stroma, while they are more isotropically distributed in the anterior two thirds, creating an interwoven and resistant net. Moving towards the limbus, the lamellae assume a circumferential orientation [2]. This highly organized structure may be altered by genetic or external factors: such structural alteration may occur as a post-surgical complication after laser refractive surgery. Disruption of corneal structure has been observed in patients affected by keratoconus, which is a corneal pathology belonging to the family of ectatic disorders.

Keratoconus is a non-inflammatory disease characterized by a gradual asymmetrical steepening and thinning of the cornea, which usually occurs in the inferior-temporal central cornea, causing a reduction of the visual acuity up to complete loss [3]. It is a bilateral condition, whose etiology is still unclear. Some environmental factors that may cause or contribute to keratoconus development are chronic eye rubbing, which induces high levels of deformation in the corneal structure, and contact lens wear [4]. It has been observed that this pathology can affect both genders and all ethnicities, but it is more common in younger patients (between 21 and 40 years old) [5].

Keratoconus histopathology has been widely analyzed in literature: it has been observed that keratocytes in keratoconic corneas are degenerated, containing much higher concentrations of proteoglycans, which also are compromised in their turn [6]. Keratocytes are essential for maintaining the ECM at homeostatic condition [7]. Thus, it has been hypothesized that the degeneration of the proteoglycans inside the keratocytes, which are located around the fibrils, may promote a

* Corresponding author.
E-mail address: bfantaci@unizar.es (B. Fantaci).

https://doi.org/10.1016/j.compbiomed.2024.108976
Received 20 May 2024; Received in revised form 17 July 2024; Accepted 30 July 2024
Available online 9 August 2024

worsening of the adhesive function of the ECM, causing the interfibrillar cross-links to break, the lamellae to slip and fiber breakage into multiple bundles. Lamellar slippage is probably due to the pressure gradient acting on the corneal posterior surface, that together with fiber breakage and volume loss may explain the bulging and thinning phenomena, typical marks of this pathology [3].

One of the main issues related to the keratoconus disease is the difficulty of an early detection. In early stages, keratoconus is defined as *subclinical* or *form-fruste* keratoconus due to the absence of symptoms, making it difficult to be detected. When the signs of keratoconus are visible, the pathology has already progressed. A non-detected subclinical keratoconus becomes a high risk factor for keratoconus development if that patient undergoes laser refractive surgery, which nowadays has become common practice to correct medium-low refractive defects [8]. One of the detectable symptoms that patients themselves notice is blurred vision caused by irregular astigmatism [5]. Therefore, corneal topography has become routine in clinical practice to analyze corneal surfaces' characteristics in doubtful cases, when the presence of keratoconus is suspected. In fact, irregular astigmatism or abnormalities in the surface curvature or in the pachymetry can be identified by means of a corneal topographer and represent clear signs of the presence of the disease. However, nowadays a standardized protocol to be followed by clinicians in order to detect keratoconus at every stage is still lacking.

Being able to fully understand keratoconus growing process could be crucial to diagnose its presence and improve prevention strategies. Finite element (FE) models represent a useful tool that may be used to mimic keratoconus pathology and investigate its behavior. There exist a few works in literature that exploited FE methods to try to reproduce keratoconic corneas in order to analyze different aspects of this pathology, from mechanical aspects to optical changes. Pandolfi et al. [9] published one of the first works on keratoconus FE modeling, where an ellipsoidal model of a keratoconic cornea was proposed, by decreasing fibers' stiffness in a localized area of the cornea, in order to analyze the mechanical behavior in comparison with an healthy model. Later, Gefen et al. [10] made a step forward, analyzing the mechanics of FE keratoconic models characterized by localized thinning and properties' degradation, introducing a basic optical analysis of the refractive power. From then on, research advances allowed to introduce patient-specific models, in order to be able to simulate corneal tissue's response to treatments to stop the progression of the disease, such as cross-linking [11,12], or to laser refractive surgeries [13]. Microstructural models, that take into account cross-links between fibrils, have also been proposed [14,15], which were able to reproduce keratoconic shapes very close to reality at homeostatic conditions.

By exploiting the versatile nature of FE models, research lately focused on trying to understand which alterations of the corneal tissue, observed with experimental imaging techniques [6,16], may trigger or be prevalent in the development of the pathology, due to the lack of knowledge about its early stage development.

It is still not clear whether this pathology is mainly caused by a decrease in fibers stiffness [17], interfibrillar cross-links breakage and consequent disorganization or if both matrix degradation and fibers breakage progress simultaneously [18,19] or if the ECM loosens its embedding function, causing lamellar slippage and fibers rupture. In any of these hypotheses, the triggering cause of these alterations is still unknown.

All the works published and discussed up to now on FE keratoconic models used an elastic formulation, where the pathology was studied by changing the material properties in a confined area and/or introducing a geometrical thinning at homeostatic conditions, that is under the action of the IOP only.

To date, growth models have not been used to investigate keratoconus pathology. These models would provide a framework that better mimics the natural progression of the pathology in terms of the structural changes that occur during the evolution of the disease. There exist, indeed, many works that presented a so-called *growth formulation* for replicating growth and remodeling processes in different biological tissues (e.g. artery, bones, etc.) [20–27] with the aim of studying tissue regeneration as a response to injury or clinical intervention, disease progression in time, tissue adaptation and so on [28].

Changes or redistribution of mass can occur in both growth and remodeling processes. They can be characteristic of normal physiological processes, but may happen also in pathological cases, such as the one of interest in this work. Being able to formulate a mathematical model of the growth process of a tissue, healthy or pathological, can be very useful to understand the physiology or physiopathology that stands behind a disease.

This work presents a novel continuum-based growth model of keratoconus. The proposed framework accounts for the structural changes occurring in the underlying tissue during the progression of the disease, as suggested by experimental observations. The resulting model may help to better understand the etiology of the behavior of this disease with the aim of improving the early diagnosis and the treatment of the pathology.

2. Materials and methods

When changes of mass are modeled in biological tissues, two main approaches can be followed, depending on the characteristics of the process itself [21]: a coupling between mass changes and deformations must be defined at the constitutive level or at the kinematic level. At the constitutive level, the free energy function is weighted with respect to the density, which can vary while the volume remains constant (mostly used in bone remodeling processes), while at the kinematic level the growth process is characterized by a volumetric mass change, while the density remains constant, usually applied to soft tissues undergoing large strains (e.g. arteries). In this work, we propose a specific application of the continuum-based growth formulation at the kinematic level, characterized by a closed system without mass generation and constant volume, to mimic keratoconus arising and progression. The entire formulation that will be described has been implemented in the framework of a user material (UMAT) subroutine in FORTRAN language.

2.1. Growth model

In the material description of soft tissues, large deformation kinematics theory is involved in the context of non linear continuum solid mechanics and, thus, such formulation will be followed in the present work [29]. In order to introduce the growth formulation, we first need to recall basic kinematics theory of a body's response to a load. Let $\mathbf{X} \in \mathcal{B}_0$ be the position of a point belonging to the body B in the initial reference configuration $\mathcal{B}_0$ at the initial time t_0 and $\mathbf{x} \in \mathcal{B}_t$ the position of the same point in the current spatial configuration $\mathcal{B}_t$ at time t. A motion $\boldsymbol{\varphi} : \mathcal{B}_0 \rightarrow \mathcal{B}_t$ is used to map the reference configuration to the current configuration, so that:

$$\mathbf{x} = \boldsymbol{\varphi}(\mathbf{X}, t). \tag{1}$$

In the theory of finite growth, first introduced by [30], a multiplicative decomposition of the deformation gradient $\mathbf{F} = \nabla\boldsymbol{\varphi} = \partial\mathbf{x}/\partial\mathbf{X}$ into a growth component $\mathbf{F}_g$ and an elastic component $\mathbf{F}_e$ (see Fig. 1) must be introduced:

$$\mathbf{F} = \mathbf{F}_e \cdot \mathbf{F}_g. \tag{2}$$

The growth component of the deformation $\mathbf{F}_g$ generates an intermediate configuration $\widehat{\mathcal{B}}_0$, that may be incompatible due to the creation of penetrations or holes among the different parts of the body, given that each particle growths independently. To ensure compatibility, an elastic deformation must be considered to maintain body's continuity. Consequently, the growth tensor $\mathbf{F}_g$ represents the change of mass in terms of addition (growth) or subtraction (degradation) of mass

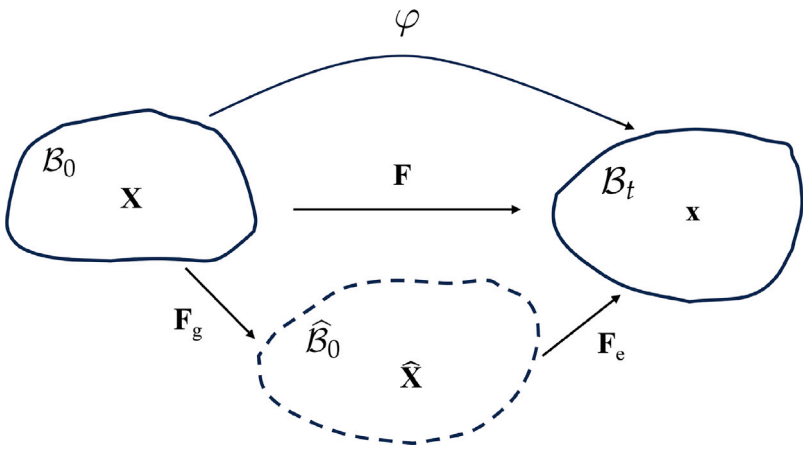

Fig. 1. Multiplicative split of the deformation gradient F.

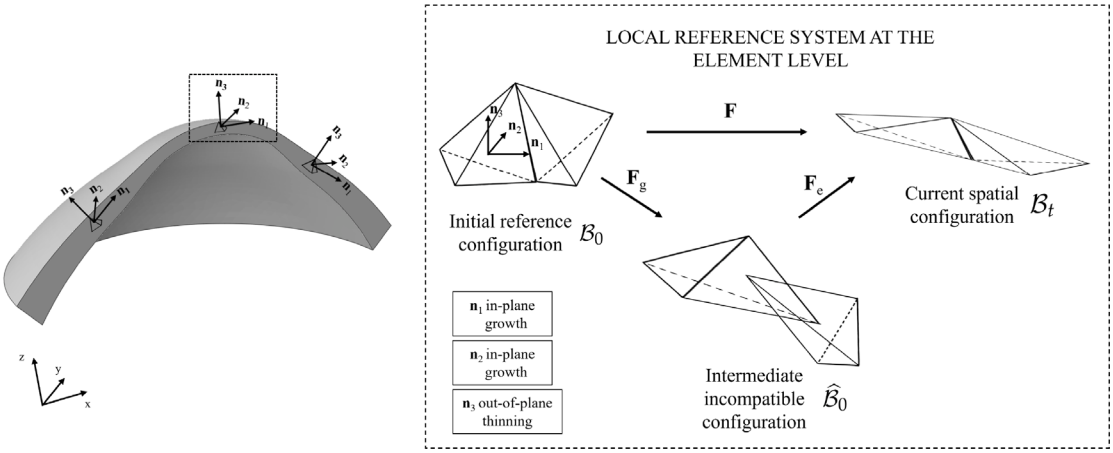

Fig. 2. Local directions of growth/degradation at the element level.

in a local volume element, while the elastic deformation gradient $\mathbf{F}_e$ accounts for the elastic deformation of the body.

As a consequence of the multiplicative split of the deformation gradient, we can define the following Jacobians:

$$J = det(\mathbf{F}) > 0, \quad J_g = det(\mathbf{F}_g) > 0, \quad J_e = det(\mathbf{F}_e) > 0, \tag{3}$$

that transform a volume element into the corresponding configurations:

$$dv = J\,dV = J_e d\hat{V}, \quad d\hat{V} = J_g dV, \tag{4}$$

where dV indicates a volume element in the initial material configuration $\mathcal{B}_0$, $d\hat{V}$ a volume element in the intermediate incompatible configuration $\widehat{\mathcal{B}}_0$ and dv a volume element in the current spatial configuration $\mathcal{B}_t$.

For the modeling of keratoconus growth, we assumed a transversely isotropic growth, composed of an in-plane isotropic growth, and an out-of-plane thinning, as a strain-driven phenomenon. Hence, a local reference system is defined at each point of the cornea (see Fig. 2), with unit vectors $\mathbf{n}_1$ and $\mathbf{n}_2$ defining a plane tangent to the corneal profile where isotropic in-plane growth occurs, and $\mathbf{n}_3$ the normal to the cornea where the out-of-plane thinning occurs. Consequently, the growth deformation gradient $\mathbf{F}_g$ can be written as:

$$\mathbf{F}_g = \vartheta\mathbf{1} + \left[\frac{1}{\vartheta^2} - \vartheta\right]\mathbf{n}_3 \otimes \mathbf{n}_3, \tag{5}$$

where ϑ is the in-plane stretch ratio. As a consequence of the selected growth formulation, the growth deformation gradient $\mathbf{F}_g$ is isochoric, respecting the incompressibility assumption made in the current model.

To start the growth process, a degradation of the corneal material properties of the constitutive model throughout time is introduced (see Section 2.3). To establish the law of evolution of growth as a strain-driven phenomenon, it is first defined the strain difference φ:

$$\varphi = \lambda - \lambda_{\text{crit}}, \tag{6}$$

where λ_{crit} is the maximum principal stretch at homeostatic conditions, that is at physiological IOP, and λ is the current stretch at time t. When $\varphi > 0$, the growth process is initiated by updating ϑ according to the explicit law:

$$\frac{d\vartheta}{dt} = \begin{cases} 0 & \text{if} \quad \varphi \le 0, \\ K^+\left(\dfrac{\vartheta_{\max} - \vartheta^t}{\vartheta_{\max} - 1}\right)^{\gamma}\varphi & \text{if} \quad \varphi > 0, \end{cases} \tag{7}$$

where $\vartheta_{\max}$ is a growth limit defined to avoid unlimited growth, K^+ and γ are two constants that regulate growth velocity. In the implementation, Eq. (7) is integrated explicitly.

2.2. Material model

Being the stroma the major constituent of corneal tissue, it is the main responsible for the mechanical response. For this reason, we chose to model corneal tissue as a tissue made up only by the stroma, disregarding the other layers, as it has already been done in others works in literature [18,31–33]. The decision to disregard the other layers has been made due to the absence of information about the mechanical behavior of such layers, even if we are aware that in

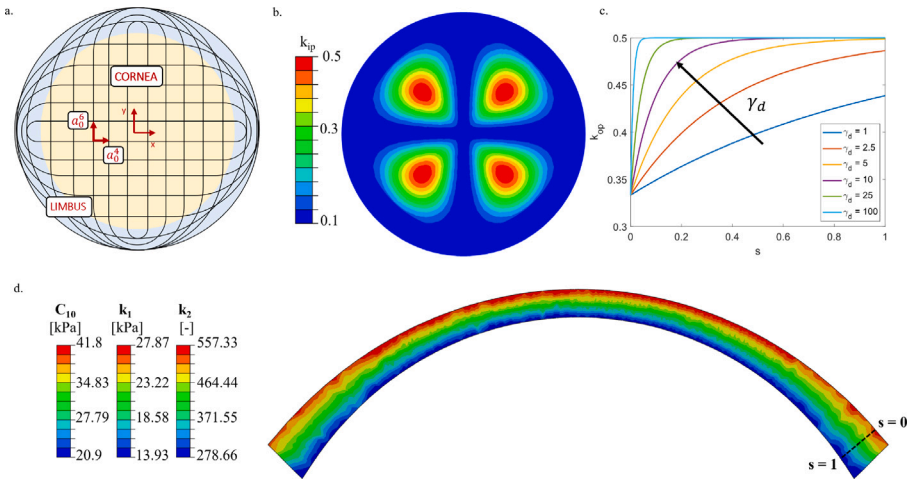

Fig. 3. Material model characteristics. a. Schematic of theoretical collagen fibers distribution, according to [36]; b. Variation of the in-plane dispersion k_{ip} in the corneal geometry; c. Variation of the out-of-plane dispersion k_{op} as a function of the local coordinate s; d. Heterogeneous distribution of material properties (C_{10}, k_1 and k_2) in corneal thickness.

keratoconus' pathology structural changes have also been observed at the epithelium and at the anterior limiting lamina.

As already underlined in the introduction of this work, collagen fibers in the stroma follow a highly organized structure [2]. The scheme of Fig. 3.a is a theoretical representation of fibers orientation, which are not perfectly aligned in the stromal tissue, but are characterized by different degrees of dispersion depending on their location in the cornea. To account for point-wise fibers dispersion, we considered in-plane and out-of-plane dispersion terms, as derived by [34,35]. In-plane dispersion follows the pattern shown in Fig. 3.b, where 0.1 is the minimum value (completely anisotropic) and 0.5 is the maximum value (completely isotropic); out-of-plane dispersion varies in depth, being the fibers more orthogonally distributed within the posterior two thirds ($k_{op} = 1/2$) and more isotropically oriented within the anterior third ($k_{op} = 1/3$).

The following strain energy density function (SEDF) for a nearly-incompressible material has been used to model the elastic part of corneal tissue behavior [35]:

$$\psi(J_e, \overline{\mathbf{C}}_e) = \psi^{matrix}(\bar{I}_1, \bar{I}_2) + \Sigma_{i=4,6}\psi^{fibers}(\overline{\mathbf{C}}_e, \mathbf{H}_i) + \psi(J_e), \tag{8}$$

where $\psi^{matrix}(\bar{I}_1)$ represents the isotropic contribution, $\psi^{fibers}(\overline{\mathbf{C}}_e, \mathbf{H}_i)$ accounts for the fibers of the model and $\psi(J_e)$ is the volumetric term.

$\overline{\mathbf{C}}_e$ is the distorsional right Cauchy–Green tensor :

$$\overline{\mathbf{C}}_e = J_e^{-2/3}\mathbf{C}_e, \tag{9}$$

where $\mathbf{C}_e = \mathbf{F}_e^T\mathbf{F}_e$ is the right Cauchy–Green tensor of the elastic part, see Eq. (2). The invariants of $\overline{\mathbf{C}}_e$ are:

$$\bar{I}_1 = tr\overline{\mathbf{C}}_e, \tag{10}$$

$$\bar{I}_2 = \frac{1}{2}(\bar{I}_1^2 - \overline{\mathbf{C}}_e : \overline{\mathbf{C}}_e), \tag{11}$$

$$\bar{I}_3 = det(\overline{\mathbf{C}}_e) = 1. \tag{12}$$

The anisotropy of the cornea is characterized by the fabric tensor $\mathbf{H}_i$, $i = \{4, 6\}$, that accounts for fibers dispersion and is defined as:

$$\mathbf{H}_i = A\mathbf{1} + B\mathbf{a}_0^i \otimes \mathbf{a}_0^i + (1 - 3A - B)\mathbf{a}_n \otimes \mathbf{a}_n, \tag{13}$$

with constants $A = 2k_{ip}k_{op}$ and $B = 2k_{op}(1 - 2k_{ip})$. The unit vectors $\mathbf{a}_0^4$ and $\mathbf{a}_0^6$ are associated with the mean preferential directions of the two families of fibers that characterize the corneal stroma (see Fig. 3.a), whereas $\mathbf{a}_n$ is the unit vector normal to the cornea, that identifies the out-of-plane direction.

The following equations for in-plane dispersion k_{ip} were used (Fig. 3.b):

$$k_{ip}(\theta) = \left(\frac{k_{ip}^{min} + k_{ip}^{max}}{2}\right) - \left(\frac{k_{ip}^{max} - k_{ip}^{min}}{2}\right) cos4\theta, \tag{14}$$

$$k_{ip}(\theta, r) = k_{ip}^{min} + \frac{1}{2}\left(k_{ip}(\theta) - k_{ip}^{min}\right)\left(1 - \cos\frac{2\pi r}{R_{TZ}}\right), \tag{15}$$

where $k_{ip}^{min} = 0.1$, $k_{ip}^{max} = 0.5$ and $R_{TZ} = 5.5$ mm is the radius of the transition zone from the cornea to the limbus.

To assign the out-of-plane dispersion k_{op}, a local coordinate $s \in [0, 1]$ was defined, parallel to the normal unit vectors. This local coordinate is 0 at the anterior surface and 1 at the posterior surface, changing throughout the corneal thickness (Fig. 3.c–d). The equation for the out-of-plane dispersion is the following:

$$k_{op}(s) = k_{op}^{min} + (k_{op}^{max} - k_{op}^{min})(1 - e^{-\gamma_d s}), \tag{16}$$

where $k_{op}^{min} = 1/3$ and $k_{op}^{max} = 1/2$ and the constant γ_d controls the non linearity of Eq. (16). Given that in the range of interest of our simulations (IOP = 0–20 mmHg), the non-linear behavior of Eq. (16) is similar for any γ_d, a value of $\gamma_d = 1$ was used.

A Neo-Hookean model was selected to describe the behavior of the matrix component of the tissue:

$$\psi^{matrix}(\bar{I}_1) = C_{10}(\bar{I}_1 - 3), \tag{17}$$

where C_{10} is a material constant which accounts for matrix's stiffness.

To model the anisotropic contribution of the collagen fibers, the hyperelastic Holzapfel–Gasser–Ogden model with dispersion parameters was used [34,35]:

$$\psi^{fibers}(\overline{\mathbf{C}}_e, \mathbf{H}_i) = \sum_{i=4,6}\frac{k_1}{2k_2}\left(e^{k_2(\bar{I}_i^* - 1)^2} - 1\right), \tag{18}$$

where k_1 and k_2 denote the fibers stiffness and fibers non-linearity, respectively. The distorsional generalized invariant $\bar{I}_i^*$ has the following form:

$$\bar{I}_i^* = \mathbf{H}_i : \overline{\mathbf{C}}_e = 2k_{ip}k_{op}\bar{I}_1 + 2k_{op}(1 - 2k_{ip})\bar{I}_i + (1 - 6k_{ip}k_{op} - 2k_{op}(1 - 2k_{ip}))\bar{I}_n, \tag{19}$$

with

$$\bar{I}_i = \overline{\mathbf{C}}_e : \mathbf{a}_0^i \otimes \mathbf{a}_0^i, \tag{20}$$

$$\bar{I}_n = \overline{\mathbf{C}}_e : \mathbf{a}_n \otimes \mathbf{a}_n. \tag{21}$$

Table 1
Corneal material parameters along the corneal thickness.

	C_{10} [kPa]	k_1 [kPa]	k_2 [–]	k_{ip}-k_{op} [–]
First layer (anterior surface)	41.8	27.87	557.33	Eqs. (15)–(16)
Second layer	34.83	23.22	464.44	Eqs. (15)–(16)
Third layer	27.786	18.578	371.55	Eqs. (15)–(16)
Fourth layer (posterior surface)	20.9	13.93	278.66	Eqs. (15)–(16)

Finally, the volumetric term is:

$$\psi(J_e) = \frac{1}{D}(\log J_e)^2, \tag{22}$$

where D is the volumetric constant.

To mimic the variation of stiffness throughout the thickness, characteristic of corneal tissue [37], we divided corneal thickness into four different layers and we assigned material properties with a linear variation from the posterior surface to the anterior, similarly to [19]. More specifically, we assigned the maximum values of the material properties at the anterior surface which gradually decrease until they reach a 50% of the initial value at the posterior surface (Fig. 3.d) [13,37–39]. We assumed a linear variation for the matrix stiffness constant C_{10}, for the fibers stiffness constant k_1 and for the constant that controls fibers non-linearity k_2. To determine the correct constant values to be assigned to each layer, an optimization process was run with the aim of obtaining the same apical displacement as the one of a homogeneous monolayer corneal model found in literature [35], which had been previously optimized with respect to experimental inflation tests [40]. The material parameters assigned to each layer of our model are shown in Table 1.

2.3. Corneal tissue degradation process

In order to correctly define the conditions that could promote keratoconus growth, some hypotheses were made. First, it was assumed that the growth process can be initiated by a local increase in the strain acting in the cornea as a consequence of the gradual reduction of stromal mechanical properties in a limited area of the cornea. If the strain does not increase in any part of the cornea, the growth process does not start.

To cause a localized strain increase, a degradation of corneal material properties was introduced: once the model is pressurized by applying a physiological IOP, the degradation process begins from a well defined area at the posterior surface (fourth layer in our model), since it is commonly believed that is the region where keratoconus starts developing [3,6,16,19] (Fig. 4.a), and progressively diffuses towards the anterior surface (first layer).

When an initial reduction Red_i of a selected material property is reached in a specific layer (in this case it was set to 10% with respect to the initial healthy value), the degradation begins in the upper layer. This process ends when the material property has decreased of a percentage Red_f (in this case 50%) with respect to its initial healthy value in each layer. The anterior layer, named as first layer, will be the last to complete the degradation.

The pathological zone that undergoes degradation is defined by a circular area of radius r_K and center C_K (Fig. 4.b). Surrounding the central area, a transition zone between the pathological and the healthy tissue, was defined. The radius of this transition zone, $r_{trans}(t)$, starting from r_K, gradually increases throughout the simulation time until reaching a final radius of $r_{healthy}$. The transition radius $r_{trans}(t)$ reaches the value of $r_{healthy}$ when the degradation process ends in each respective layer.

The material degradation of the pathological area and the expansion of the transition zone throughout time were defined according to a space–time-dependent sigmoid function:

$$X(r,t) = \begin{cases} X_i & \text{if} \quad t < t_i \\ X_i + (X_f - X_i)(10 - 15\Delta t + 6\Delta t^2)\Delta t^3 \alpha(r,t) & \text{if} \quad t_i \le t \le t_f \\ X_f & \text{if} \quad t > t_f \end{cases}$$

where

$$\Delta t = \frac{t - t_i}{t_f - t_i}$$

is the time increment and t is the value of total simulation time at the time increment Δ t; t_i is the initial degradation time of a specific layer, that is the time when a reduction Red_i = 10% has been reached in the previous layer, excluding the posterior surface layer, where $t_i = 0$ since it is the first layer to degrade; t_f is the final degradation time of the same layer (set as $t_f = t_i + 1$). $X(r,t)$ is the degraded material parameter at time t and radius r, X_i is the initial healthy value of the parameter of interest before the degradation starts, i.e. the healthy value, and X_f is the final value when the degradation ends, i.e. the pathological value characterized by a reduction Red_f = 50%; α(r,t) is a constant that varies between 0 (healthy zone) and 1 (pathological zone), needed to assign a linear variation of the parameters in the transition zone, as $r_{trans}(t)$ increases throughout the degradation process due to the pathology progression. It is defined as

$$\alpha(r,t) = \frac{r_{trans}(t) - r}{r_{trans}(t) - r_K} \tag{23}$$

where r_K is the radius of the completely degraded zone;

$$r_{trans}(t) = r_K + (r_{healthy} - r_K)\Delta t \tag{24}$$

is the radius of the transition zone at time t that is linearly increasing, as the degradation progresses, and $r_{healthy}$ is the final radius where the transition zone ends and the healthy tissue starts.

In Fig. 5, we show some examples of material constants degradation throughout time in the central keratoconic area (left) and in the transition zone (right), by considering points in the transition zone at different distances with respect to the center of the pathological area.

2.4. FE model, simulation set-up and conducted analyses

A 3D conic geometry [41] with average dimensions (anterior surface: apical radius R_{AS} = 7.56 mm and asphericity Q_{AS} = −0.19; posterior surface: apical radius R_{PS} = 6.20 mm and asphericity Q_{PS} = −0.14; central corneal thickness: CCT = 564 μm) was used to build the FE corneal model. Model's surfaces point clouds were built by means of a MATLAB code and directly meshed with quadratic tetrahedrons of 0.1 mm dimension with the software ANSA version 22.0.1 by BETA CAE Systems. The mesh sensitivity of the proposed FE model was conducted in a previous work from our group, where both mechanical and optical accuracy were analyzed (see Figure 6 in [41]). Fixed boundary conditions were assigned to the base of the cornea and a physiological IOP of 15 mmHg [42] was applied to the posterior surface of the cornea, mimicking the action of the humors inside the eyeball cavity. To recover the initial unloaded geometry, the zero-pressure algorithm from [43] was used. The stress-free geometry becomes the initial geometry for our simulation, made of two steps: first, the model is pressurized with the IOP, defined as homeostatic condition; in the second step, a localized degradation of corneal tissue properties is initiated and, if the strain increases with respect to homeostatic conditions, the growth process starts.

Three analysis were performed, using the software ABAQUS 2022, to analyze different aspects of the pathology and parameters of the numerical model.

The first analysis aimed at understanding how each material parameter of the numerical model contributed to the growth process.

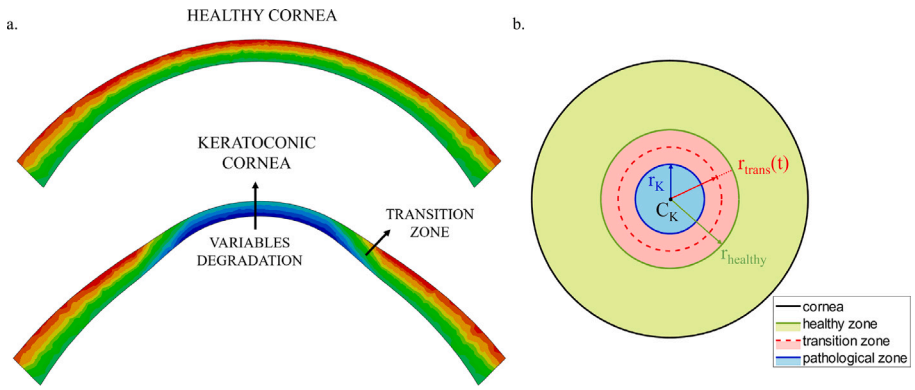

Fig. 4. Schematic of the degradation process of corneal tissue. a. Comparison between healthy corneal material properties and degraded material properties in the keratoconic cornea; b. Schematic of the different zones of interest in the model (pathological, transition and healthy).

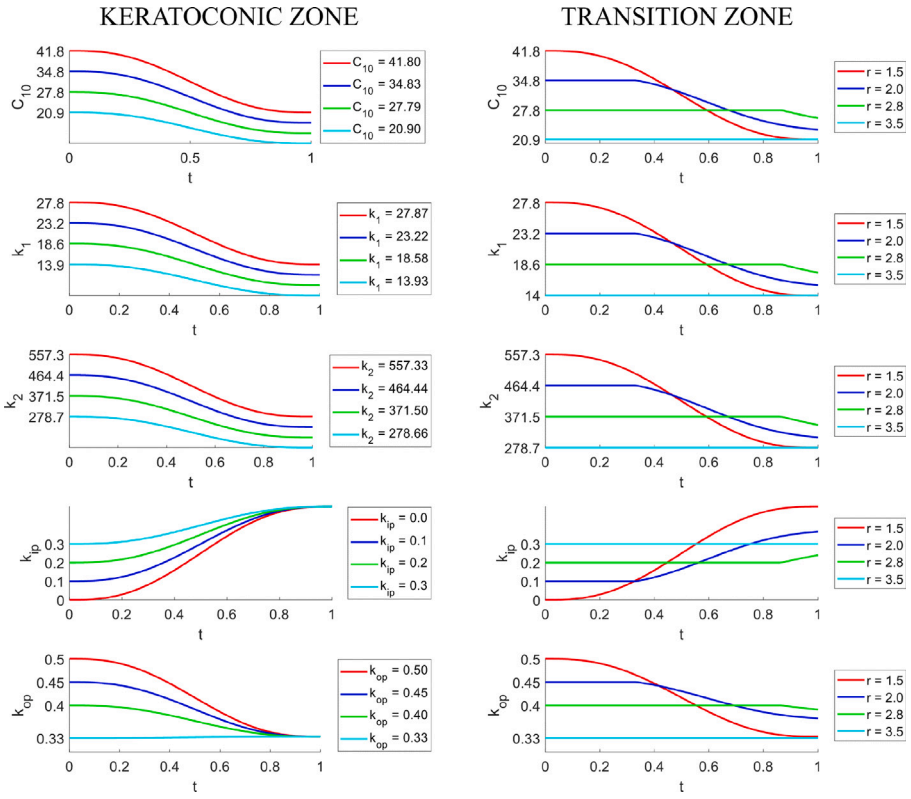

Fig. 5. Material parameter degradation in the keratoconic and in the transition zones. In this example r_K = 1.5 mm and $r_{healthy}$ = 3 mm, t = 0 and t = 1 are the initial and final degradation times, respectively. Left: material parameters degradation in the keratoconic zone, depending on the initial healthy value of the material parameter of interest, belonging to a specific layer; right: material parameters degradation of points in the transition zone (r = 2, 2.8 mm), at the boundary of the pathological zone (r = 1.5 mm) and in the healthy zone (r = 3.5 mm), characterized by different initial constants values depending on the layer of interest.

To do so, one parameter of the SEDF (Eq. (8)) at a time was degraded: extracellular matrix stiffness (C_{10}), fibers stiffness (k_1), fibers non-linearity (k_2), in-plane and out-of-plane dispersions (k_{ip} and k_{op}). Constants C_{10}, k_1 and k_2 were degraded until they reached the 50% of their initial healthy value [44], while dispersion parameters k_{ip} and k_{op} were changed until reaching their isotropic limit, 0.5 and 0.33, respectively, given the disorganization of collagen fibers, typically observed in keratoconic corneas [16]. In this first analysis, the degraded zone was placed at the center of the cornea (C_K = [0,0]).

The second analysis consisted in degrading all variables simultaneously. Even if it is still not clear in which order the different tissue components may undergo a loss of their mechanical properties or if the degradation process of different tissue components takes place simultaneously, due to the lack of experimental proof, it is likely that at some point of the pathology different processes coexist and progress. For this reason, the sum of the contributions of the degradation of all material parameters (C_{10}, k_1, k_2, k_{ip} and k_{op}) was evaluated. For this analysis, an off-center case was considered, as keratoconus most-likely develops in the infero-central region of the cornea. Consequently, the center C_K of the pathological zone that undergoes degradation during the simulation was placed at coordinates x = −0.663 mm and y = −1.019, as indicated by [45], considering the Pentacam topographer reference system. Material constants (C_{10}, k_1 and k_2) were degraded until reaching the 50% of their initial healthy value and dispersion parameters (k_{ip} and k_{op}) until reaching their isotropic limit.

In the first and second analysis, the radius of the pathological zone r_K was set as 1.5 mm and the maximum radius of the transition zone was set as 3 mm, which coincides with the beginning of the healthy

Table 2
Evolution of keratoconus severity evaluated with Belin grading system throughout the simulation time when the degradation of each material parameter occurs at a time.

Time	Extracellular matrix C_{10}				Dispersions k_{ip}-k_{op}			
percentage [%]	$K_{m\ AS}$ [D]	$K_{m\ PS}$ [D]	Thinnest pachymetry [μm]	Belin ABCD	$K_{m\ AS}$ [D]	$K_{m\ PS}$ [D]	Thinnest pachymetry [μm]	Belin ABCD
0	44.59	54.38	564.80	A0, B0, C0	44.59	54.38	564.80	A0, B0, C0
10	45.77	55.71	556.13	A0, B0, C0	44.86	54.73	562.45	A0, B0, C0
20	61.61	73.73	472.46	A4, B4, C1	46.55	56.40	552.45	A1, B0, C0
30	72.20	86.85	410.45	A4, B4, C2	48.18	57.40	542.65	A2, B1, C0
40	76.20	90.63	390.15	A4, B4, C3	50.66	61.91	523.54	A2, B2, C0
50	77.76	91.54	382.55	A4, B4, C3	53.33	72.41	489.83	A3, B4, C1
60	78.47	91.79	379.63	A4, B4, C3	57.42	84.64	463.59	A4, B4, C1
70	78.90	91.97	378.51	A4, B4, C3	61.89	95.32	445.94	A4, B4, C2
80	79.19	92.15	378.06	A4, B4, C3	65.37	102.46	434.93	A4, B4, C2
90	79.40	92.31	377.87	A4, B4, C3	67.42	106.18	428.13	A4, B4, C2
100	79.55	92.44	377.78	A4, B4, C3	68.86	107.36	422.50	A4, B4, C2
Time	Fibers stiffness k_1				Fibers non-linearity k_2			
percentage [%]	$K_{m\ AS}$ [D]	$K_{m\ PS}$ [D]	Thinnest pachymetry [μm]	Belin ABCD	$K_{m\ AS}$ [D]	$K_{m\ PS}$ [D]	Thinnest pachymetry [μm]	Belin ABCD
0	44.59	54.38	564.80	A0, B0, C0	44.59	54.38	564.80	A0, B0, C0
10	44.67	54.49	563.98	A0, B0, C0	44.60	54.41	564.50	A0, B0, C0
20	45.50	55.21	559.29	A0, B0, C0	44.88	54.59	563.11	A0, B0, C0
30	46.07	55.58	554.94	A0, B0, C0	45.12	54.62	561.97	A0, B0, C0
40	46.73	56.46	546.14	A1, B0, C0	45.46	54.76	559.41	A0, B0, C0
50	50.74	59.70	514.98	A2, B2, C0	47.14	54.56	547.55	A1, B0, C0
60	58.70	69.40	472.86	A4, B4, C1	53.00	57.12	510.83	A3, B0, C0
70	64.28	77.43	446.75	A4, B4, C2	60.78	64.89	469.22	A4, B2, C1
80	67.24	82.32	433.30	A4, B4, C2	65.05	71.08	446.18	A4, B4, C2
90	69.13	84.78	424.72	A4, B4, C2	67.46	75.06	434.68	A4, B4, C2
100	70.47	85.64	419.95	A4, B4, C2	69.22	77.34	428.58	A4, B4, C2

zone, as in [9]. This last zone goes from a radius $r_{healthy}$ of 3 mm to the whole corneal radius (r_{cornea} = 6 mm).

The third analysis focused on studying the influence of the dimension and the position of the affected pathological area on the growth. To do so, two models were used, one where the pathological zone was placed at the corneal center and the other where the pathological zone was off-center, as in the previous analysis (C_K = [−0.663, −1.019]). For each model, four cases with different radii of the keratoconic zone (r_K = 0.5 mm, 1 mm, 2 mm and 3 mm) were considered; for each case, the maximum transition radius, which again coincides with the beginning of the healthy zone ($r_{healthy}$), was set as the double of the value of r_K. In this analysis, material degradation was set equal to the previous ones.

In all analysis the constants K^+ and γ, that controls growth velocity (Eq. (7)), were set as 5 and 1, respectively; these values were chosen arbitrarily, due to the lack of information on keratoconus growth velocity and due to the fact that the time of the pathology development can highly vary from one patient to another. To avoid unlimited growth, the growth limit ϑ_{max} was set as 1.20.

2.5. Keratoconus evolution

To evaluate keratoconus evolution in the model throughout time, the Belin ABCD keratoconus staging system [46], which is the classification currently used in the Pentacam topographer by Oculus Optikgeräte GmbH (Wetzlar, Germany), was considered. This staging system assigns a keratoconus severity grade, based on four parameters (ABCD): parameter A is the curvature at the anterior surface in a zone of 3 mm centered on the thinnest pachymetry ($K_{m\ AS}$ in Tables 2–4); B is the curvature at the posterior surface in a zone of 3 mm centered on the thinnest pachymetry ($K_{m\ PS}$); C is the thinnest pachymetry point in μm and D is distance best corrected visual acuity, that is patient's subjective refraction. Depending on the resulting values, five different stages for classifying keratoconus can be assigned.

In the current work, an algorithm that computed the same parameters (ABC) was developed. More in details, parameters A and B were computed as the tangential curvature of the center of the cone at the anterior and posterior surfaces respectively; the center of the cone is known in the model, since it is the center of the degraded zone; tangential curvature was computed by performing a sphere fitting at each point of the anterior surface [47]. Parameter C was evaluated by finding the minimum normal distance between the anterior and posterior surface nodes. Parameter D was not included in the study as it is not machine generated and depends on patient's subjective refraction.

3. Results

In the following sections, we first present the results of the material sensitivity analysis on the parameters that may influence the growth process; then, we report a more realistic case where all the parameters considered in the first analysis are degraded at once and, finally, an analysis on the dimension and the position of keratoconus is presented.

3.1. Influence of material parameters degradation on keratoconus growth. single-effect analysis

In this analysis, the effect of the degradation of a single material parameter on keratoconus growth was analyzed. Fig. 6 shows the distribution of in-plane growth component of the deformation gradient in the corneal section at different time frames when the degradation of the material parameters occurs individually. Fig. 7.a shows the time evolution of $\mathbf{F}_{g\ \text{in-plane}}$ for each material parameter that degrades, while Fig. 7.b shows the time evolution of the material parameters that undergo degradation.

The major contribution to the growth is given by the ECM stiffness (C_{10}), whose degradation causes the cone to grow faster (Fig. 7.a) with the pathological zone quickly reaching the growth limit ϑ_{max}. The loss of mechanical properties of the ECM causes the formation of a symmetrical isotropic cone which turned out to be the most severe among the four cases considered (Table 2). The other mechanical parameters (fibers stiffness, k_1; fibers non-linearity, k_2; and loss of fibers' orientation, k_{ip} and k_{op}) cause a more gradual non-homogeneous growth, which generates an anisotropic and less symmetric cone, that does not entirely reach the growth limit (Figs. 6–7.a).

Table 2 and Fig. 8.a–c show the evolution throughout time of cone severity according to the Belin grading system: while matrix degradation causes the cone to bulge out very rapidly, passing quickly from grade 0 to grade 3–4 of severity and reaching the thinnest pachymetry among all cases, the fibers parameters generate a more gradual cone,

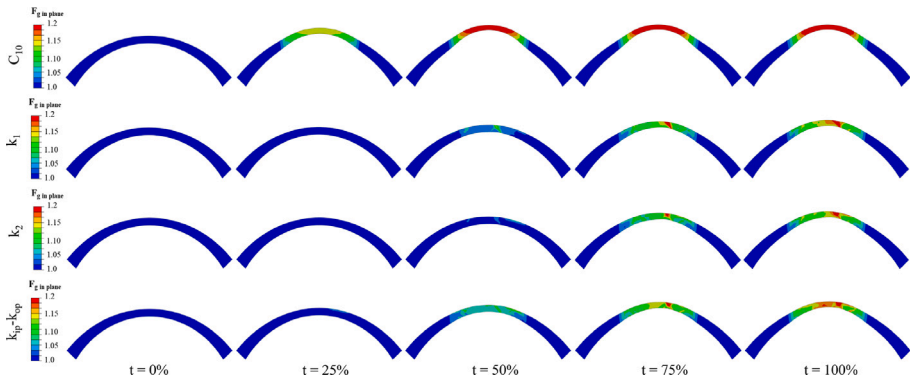

Fig. 6. In-plane growth at different time percentages of the simulation, caused by degrading one material parameter at time.

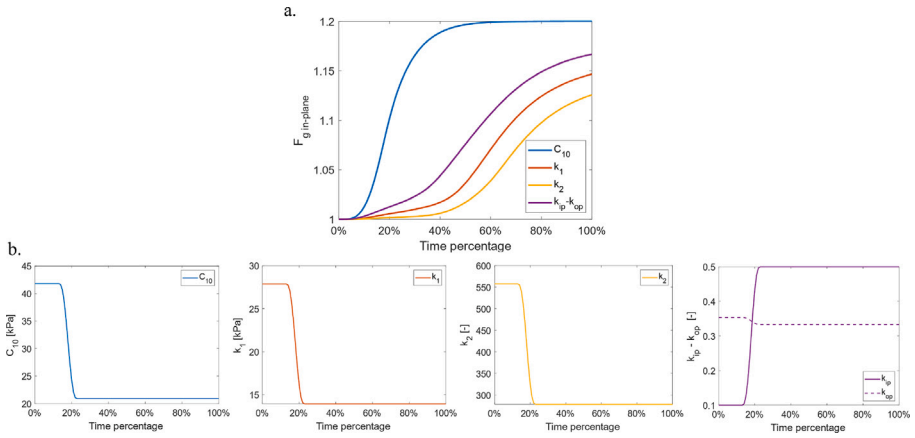

Fig. 7. a. Time evolution of the in-plane growth component of the deformation gradient F_g for each case for a point belonging to the anterior surface, which is the last to degrade; b. Degradation of the material parameters of a point belonging to the anterior surface.

whose severity increases in a slower way throughout time, gradually passing from all the grades classified by Belin grading system. After matrix degradation (C_{10}), the second more influential parameters that seem to affect keratoconus growth are the fibers in-plane and out-of-plane dispersions (k_{ip} and k_{op}), by causing the cone to grow faster after they reached their isotropic limits (Fig. 7.a–b); more specifically, the disorganization of fibers orientation seems to be the mechanism that mostly affects the posterior surface curvature in the keratoconic zone (Fig. 8.b), while the anterior surface curvature and the pachymetry seem to be affected in a similar manner by all the fiber parameters considered in this study (Fig. 8.a and c).

Lastly, the less important contribution to the growth is given by the parameter that controls fibers' non-linearity (k_2), which causes the largest delay in triggering keratoconus growth (Figs. 7.a–8). Interestingly, the results indicate that the effect that k_1, k_2 and the dispersion parameters k_{ip} and k_{op} have on the anterior surface and on the pachymetry is the same besides the fact that k_2 activates keratoconus growth later. The largest difference in terms of the influence of the parameters on the final cone shape can be observed at the posterior surface (Fig. 8.b), where each parameter contributes differently on the final curvature value (parameter B, Table 2).

In general, while the degradation of the matrix rapidly affects keratoconus growth, with consequences already noticeable when the tissue is still degrading, for the other parameters, keratoconus growth is only noticeable after they have fully degraded (reaching their degradation limit, $Red_f = 50\%$), (Figs. 7–8).

In all cases, the model was able to closely reproduce a keratoconic cornea of growing severity with the characteristic bulging and thinning, by degrading a single material parameter.

Table 3
Evolution of keratoconus severity evaluated with Belin grading system throughout the simulation time, when all the material variables degrade simultaneously.

Time percentage [%]	Km AS [D]	Km PS [D]	Thinnest pachymetry [μm]	Belin ABCD
0	44.31	54.26	564.80	A0, B0, C0
5	44.29	54.31	564.18	A0, B0, C0
10	46.26	57.33	553.10	A0, B1, C0
15	54.38	66.89	514.98	A3, B3, C0
20	65.98	81.40	454.73	A4, B4, C1
25	73.70	89.70	410.98	A4, B4, C2
30	77.22	92.57	392.15	A4, B4, C3
35	78.86	93.58	383.56	A4, B4, C3
40	79.70	93.96	379.54	A4, B4, C3
45	80.18	94.17	377.67	A4, B4, C3
50	80.47	94.29	376.79	A4, B4, C3

3.2. *Influence of the degradation of all material parameters on keratoconus growth. Off-center case*

For this analysis, an off-center cone was obtained by degrading all material properties at once in the inferior-temporal region, where keratoconus most likely develops. The evolution of the cone, when the degradation of all mechanical properties occurs, is shown in Fig. 9 and Table 3.

When all the material variables degrade simultaneously, a very severe cone already develops at half of the total simulation time. As the pathology progresses, the thinnest pachymetry point displaces towards the center of the pathological zone (Fig. 9, bottom). The keratoconic shape obtained in this off-center analysis is usually classified as oval cone, which is the most diffused form of keratoconus.

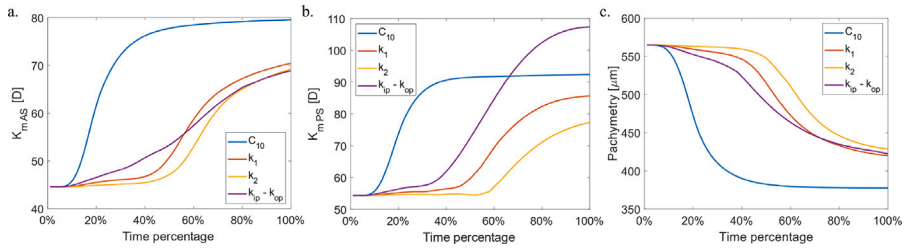

Fig. 8. Time evolution of the anterior (a.) and posterior (b.) surface curvature at the center of the pathological zone (parameters A and B in Belin grading system, respectively) and of the thinnest pachymetry point (c.) (parameter C in Belin grading system) for each material parameter.

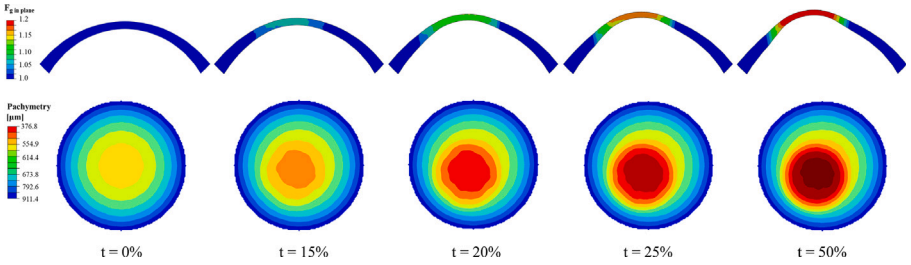

Fig. 9. Top: In-plane growth at different time percentages of the simulation, caused by degrading all the variables simultaneously; bottom: pachymetry thinning at different time percentages of the simulation.

3.3. Keratoconus dimension and position analysis

In this last analysis, the influence of the dimension and the position of the pathological zone was analyzed. Fig. 10 shows the in-plane component of the growth deformation gradient $\mathbf{F}_g$ for both centered and off-center cones at increasing r_K. As it can be observed, the dimension of the affected pathological zone appears to have a high influence on the final cone shape. For the cases with smaller radius (r_K = 0.5 and 1 mm) a sharp asymmetric cone was obtained, which mimics the keratoconus form named as *nipple cone*. The case with radius r_K = 2 mm closely mimics the so-called *oval cone*, which is the most diffused form of keratoconus, also obtained with the model of the previous analysis, characterized by a r_K = 1.5 mm. In this type of keratoconus the bulging area is larger with respect to the previous two cases (r_K = 0.5 and 1 mm) and usually develops in the inferior-temporal cornea, which is closely reproduced by the off-center case of radius r_K = 2 mm. The latter case with r_K = 3 mm represents the most severe but also most uncommon form of keratoconus named as *globus cone*, where the bulging affects almost the entire cornea. The location of the cone affects the results in terms of reproducing more closely real cases depending on the zone where each type of cone most-likely develops, but it does not seem to greatly influence the growth. In fact, the centered and off-center cases are quite similar in terms of growth gradient distribution (Fig. 10) and severity based on Belin classification (Table 4). Differently from what observed in the previous analyses, where a cone of radius r_K = 1.5 mm was considered, in this analysis it turned out that, when the degraded region is smaller (r_K = 0.5 and 1 mm), the growth limit is not achieved in the whole pathological volume, suggesting that in these cases a more anisotropic growth occurs and the effect of matrix degradation does not prevail as in larger cones (r_K = 1.5, 2 and 3 mm). Table 4 classifies the severity of the analyzed cases according to Belin grading system. For both centered and off-center models, cases with radius r_K = 2 and 3 mm may appear to be less severe in terms of anterior and posterior curvatures ($K_{m\ AS}$ and $K_{m\ PS}$, parameters A and B, respectively) in the 3 mm zone of the pathological area with respect to the cones of radius r_K = 0.5 and 1 mm. This result could bring to a wrong evaluation of cone severity, if we based it only on parameters A and B; in fact, due to the bigger bulging area, the curvature in the 3 mm zone of the pathological area decreases, due to a central flattening of both anterior and posterior surfaces. This phenomenon can be observed qualitatively in Fig. 10. Moreover, it is confirmed by parameter C in Table 4, where the thinnest pachymetry is measured in the two bigger cones of radius r_K = 2 and 3 mm.

4. Discussion

The mechanisms and biological processes behind the development of keratoconus remains largely unknown to date. These processes are the responsible for the progressive bulging and thinning, typical of keratoconic corneas. Alterations in keratoconic corneas have been associated with differences in the expression of several corneal proteins that result in changes in the structural integrity of the stroma, through altering its collagen content and the degeneration of the proteoglycans around the stromal collagen fibril,s leading to breakage of collagen fibers [3]. These changes lead to alterations in the strain field induced by physical stress from the IOP that may exacerbate the degradation. In this work, a novel formulation for the reproduction of keratoconus based on a strain-driven isochoric tissue growth model is proposed. Growth is triggered by the increase in strain with respect to the homeostatic conditions following material degradation. The proposed model, and mathematical models in general, may be helpful in better understanding the mechanisms behind the formation of keratoconus, as it allows investigating the influence that multiple factors, and their interaction, have on the development of the disease.

Different authors already underlined the importance of the strain in activating cells response to maintain and remodel the ECM. Keratocytes are able to react to strain changes, activating a mechanobiological response to reestablish the homeostatic conditions in terms of tension acting in the matrix [7]. Dupps et al. [13] selected the maximum principal strain as metric to compare normal and keratoconic corneas in FE simulations of laser refractive surgeries and found a significant difference between the two cases in terms of strain distribution. Later, Kwok et al. [48], using high-frequency ultrasound elastography, measured high differences in strain between normal and keratoconic human donors corneas in the cone region, suggesting that the pathology seems to be associated with local mechanical weakening. In addition, as explained in [49], physiological strain levels (below a 3%) are essential to maintain a normal keratocytes phenotype, whereas larger magnitude strains (above 15%) contribute to ECM disorganization. Recent biochemical and immunohistochemical data support the hypothesis that

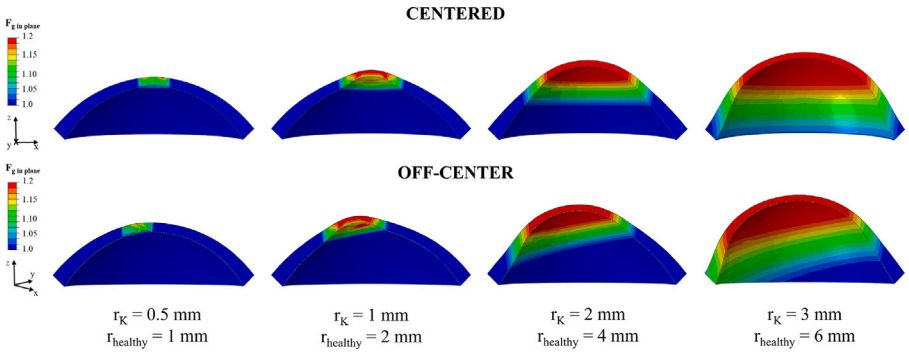

Fig. 10. Centered (top) vs. off-center (bottom) in-plane growth at the end of the simulation with varying radius of the pathological area.

Table 4
Keratoconus severity in centered and off-center cases, evaluated with Belin grading system at different dimensions of the pathological zone.

r_K [mm]	Centered				Off-center			
	Km AS [D]	Km PS [D]	Thinnest pachymetry [μm]	Belin ABCD	Km AS [D]	Km PS [D]	Thinnest pachymetry [μm]	Belin ABCD
0.5	77.63	115.81	486.50	A4, B4, C1	82.99	147.07	472.17	A4, B4, C1
1	115.08	138.75	402.83	A4, B4, C2	116.85	138.26	403.04	A4, B4, C2
2	65.55	73.99	358.61	A4, B4, C3	65.63	75.01	361.98	A4, B4, C3
3	52.90	58.36	341.50	A2, B1, C3	53.02	59.50	344.14	A3, B2, C3

alteration of various corneal proteins cause oxidative damage that lead to degradation of the stromal tissue [3,50]. Based on this evidence, our model assumes that keratoconus development starts with material degradation in a region of interest. This material degradation causes localized alterations in the strain field that triggers corneal growth and the development of keratoconus.

The choice of a strain-driven model is purely based on what has been proposed in the literature [3,13]. However, the model can be easily adapted to consider stress as the main driving force or the keratoconus growth process.

As already emphasized, a transversely isotropic growth was assumed. This choice was due to the need of establishing the simplest way to mimic the keratoconus development, given the current lack of experimental evidence on the specific progression of such disease. In this regard, an isochoric growth law was selected, where the volume was kept constant. In a transversely isotropic growth the tissue grows isotropically in the plane of the element, that corresponds to the tangent plane of the corneal profile. The same amount of 'in plane growth' is lost in the normal (out-of-plane) direction in order to obtain the thinning, typical of keratoconic corneas, while keeping the volume constant. The growth rate is thus established so that it is ensured that the growth deformation gradient is isochoric, given that the finite-element formulation is incompressible. Moreover, it is not clear whether there is a change in volume or not in keratoconus disease, but the assumption of an isochoric incompressible formulation was dictated by the fact that the cornea is highly hydrated and, thus, most-likely incompressible.

In this study the influence of different material components was investigated, in order to analyze how each single parameter affected the growth. From the first analysis, the ECM turned out to play a crucial role in cone development and pathology's progression. By degrading the ECM alone, the most severe cone was obtained, characterized by a symmetric shape, due to the fact that the loss of ECM stiffness generated a more isotropic growth. In this case, an oval cone was obtained: this represents the most common keratoconus shape, characterized by a large bulging area. For sake of simplicity, in the first analysis the area that undergoes degradation was placed at the center of the cornea, but this kind of cone usually develops in a infero-temporal zone, as it was later obtained in the second analysis of the current work.

The degradation of the fibers parameters (k_1, k_2, k_{ip} and k_{op}) also generated a severe cone according to Belin grading system (Table 2), but smaller with respect to the case where the ECM undergoes degradation. In fact, when fibers components are degraded, parameter C of Belin classification, representing corneal thinning achieves a grade 2 of severity, thus reaching a milder state with respect to the ECM degradation, characterized by a much higher thinning at the end of the simulation (C3 of severity). Contrary to the isotropic growth caused by matrix degradation, when a parameter related to the collagen fibers was degraded, an anisotropic growth was achieved, without entirely reaching the growth limit (Fig. 6). More in detail, the second most influential parameter in the growth process turned out to be the loss of fibers' orientation due to the change of the dispersion parameters (k_{ip} and k_{op}) towards their isotropic limit. As a consequence, fibers' disorganization is another factor that highly influences the growth process and that was observed in keratoconic corneas [6,16].

With the presented analyses, it was not possible to establish the chronological/causal order in which different phenomena occur during the degradation and consequent growth process. It could be hypothesized that an alteration of ECM synthesis due to a localized strain increase may cause the degradation process to prevail and, consequently, reducing the ECM functionality in keeping lamellae tightly embedded in the matrix. As a consequence, interfibrillar crosslinks breakage may occur and lamellar slippage may bring to fibers breakage, as also hypothesized by [6]. However, further analyses should be performed to address which corneal tissue constituent initiates the process of the structural disorganization, affecting the other components of the tissue, which in turn trigger the initiation of the pathology, or if more processes happen simultaneously.

Even if the causal order of phenomena observed in keratoconus histopathology is still not well understood, it is likely that as the pathology progresses some processes may coexist. With this hypothesis, the second analysis of this work was conducted, by setting the simultaneous degradation of all material parameters considered in this study in an off-center case. As anticipated above, the most diffused form of keratoconus named as oval cone was obtained, closely mimicking real keratoconic corneas.

In the last analysis of the current work, the influence of the dimension and the position of the pathological zone on the final cone was evaluated. Surprisingly, for smaller pathological zones (r_K = 0.5, 1 mm) an asymmetric anisotropic cone was obtained, where the growth limit was not reached, suggesting that the degradation of the ECM, which mostly control the isotropic behavior of the corneal material model,

did not prevail as for bigger affected areas (r_K = 1.5, 2, 3 mm). This result suggested that the ECM actually plays a major role in keratoconus development when the area that undergoes degradation covers at least half of the cornea (including the transition zone), as in the case of oval and globus cones. In these forms of keratoconus, the shape is more symmetric, indicating the higher isotropic contribution to the growth given by the ECM. In smaller cones (r_K = 0.5, 1 mm), as in the case of the nipple cone, the anisotropic components of the material model seem to prevail, contributing more to an anisotropic growth of the cone.

The position of the pathological area appears to have a lower influence on the final cone severity with respect to the dimension, as no differences were detected between centered and off-center models (Table 4).

Another aspect still debated in literature is whether the structural changes observed in pathological corneal tissue initiate from the posterior surface and propagate towards the anterior or the opposite. As other authors already did [6,16,19], we hypothesized that a loss of mechanical properties begins in a localized region at the posterior surface and propagates towards the anterior surface throughout time. The results obtained with the proposed model confirm this hypothesis, as the growth process, initiated by means of a localized material degradation at the posterior surface that gradually propagates towards the anterior, replicate very closely real keratoconic cases by obtaining different cone shapes.

All the previous works, that investigated keratoconus development and behavior by means of finite-element methods [9–19], analyzed whether the corneal model manifested bulging and thinning, with the aim of reproducing pathological conditions, by introducing a localized material stiffness reduction at homeostatic conditions (under the action of the IOP) or a geometrical thickness reduction or both, using a purely elastic formulation. The main novelty of our work lays in the proposed formulation: thanks to the introduction of the multiplicative decomposition of the deformation gradient, we take into account both elastic and growth deformations. Consequently, a permanent deformed state is obtained due to the mass redistribution at constant volume introduced by the growth component of the deformation gradient. When a purely elastic formulation is used, the symptoms of the pathology like the cone shape and the thinning, achieved at homeostatic conditions, are lost when the IOP is removed. Thus, the purely elastic formulation is not able to entirely reproduce structural changes of mass that actually characterize keratoconus pathology. Moreover, differently from works where the thinning phenomenon was absent [9,17] or early-stages of the pathology were achieved [19], due to the limits of the purely elastic formulation, we were able to reproduce all the stages of the disease, according to Belin grading system, thanks to the introduction of a growth formulation.

However, this study represents only the first step towards a deeper understanding of keratoconus disease and allows to exploit the advantages of a growth formulation to analyze separately different aspects of the pathology. Therefore, it is not exempt from limitations. First, the model only considered a one-way coupling between material degradation and corneal growth i.e., corneal growth is triggered by material degradation but corneal growth does not affects material degradation. A more realistic model should incorporate a two-way coupling between material degradation and growth. In this first study, patient-specific data were not included, as a simple conic geometry was used to test the proposed formulation. In the future, a key aspect would be to validate the methodology with patient-specific data of keratoconus evolution throughout time, although we are aware of the difficulty in recruiting such data as the clinicians intervene to stop pathology's progression before it reaches a high severity grade. Nevertheless, we believe that this new approach to investigate keratoconus pathology has already shown promising results, closely mimicking real cases. Therefore, the proposed model may help to better understand the underlying mechanisms associated with the pathology's development and worsening of the keratoconic eye. Being able to qualitatively mimic keratoconus evolution in time, the presented model could be used to test the effect of different treatments, like cross-linking treatment or intrastromal ring insertion, and may help the surgeons in selecting the most appropriate procedure, given the unpredictability of current available treatments, that often leave the patient unsatisfied with the result.

5. Conclusions

A novel formulation able to reproduce corneal keratoconus growth has been presented, which allows to investigate processes that may contribute to the pathology arising and progression. With corneal growth triggered by corneal stroma degradation, the model is able to reproduce typologies of keratoconus associated with the degradation of different components of the stroma, and the size and location of the damaged tissue. Besides its limitations, the proposed model provides a tool that allows a better understanding of the pathology, offering new opportunities to better analyze patient-specific pathological data.

CRediT authorship contribution statement

Benedetta Fantaci: Writing – review & editing, Writing – original draft, Visualization, Software, Methodology, Investigation, Formal analysis, Data curation, Conceptualization. **Begoña Calvo:** Writing – review & editing, Validation, Supervision, Methodology, Funding acquisition, Conceptualization. **José Félix Rodríguez:** Writing – review & editing, Validation, Supervision, Methodology, Conceptualization.

Declaration of competing interest

The authors declare that the research was conducted without any commercial or financial relationships that could be construed as a potential conflict of interest.

Acknowledgments

This project has received funding from the European Union's Horizon 2020 research and innovation program under the Marie Skłodowska-Curie grant agreement No 956720 and the Department of Industry and Innovation (Government of Aragon), Spain through the research group Grant T24–23R (cofinanced with Feder, Spain 2014–2020: Construyendo Europa desde Aragón). Part of the work was performed by the ICTS "NANBIOSIS" specifically by the High Performance Computing Unit (U27), of the CIBER in Bioengineering, Biomaterials and Nanomedicine (CIBER-BBN at the University of Zaragoza).

References

[1] M.S. Sridhar, Anatomy of cornea and ocular surface, Indian J. Ophthalmol. 66 (2018) 190–194, http://dx.doi.org/10.4103/ijo.IJO-646-17.

[2] M. Winkler, D. Chai, S. Kriling, C.J. Nien, D.J. Brown, B. Jester, T. Juhasz, J.V. Jester, Nonlinear optical macroscopic assessment of 3-d corneal collagen organization and axial biomechanics, Invest. Ophthalmol. Vis. Sci. 52 (2011) 8818–8827, http://dx.doi.org/10.1167/iovs.11-8070.

[3] J. Santodomingo-Rubido, G. Carracedo, A. Suzaki, C. Villa-Collar, S.J. Vincent, J.S. Wolffsohn, Keratoconus: An updated review, Contact Lens Anterior Eye 45 (2022) http://dx.doi.org/10.1016/j.clae.2021.101559.

[4] G. Ferrari, P. Rama, The keratoconus enigma: A review with emphasis on pathogenesis, Ocular Surf. 18 (2020) 363–373, http://dx.doi.org/10.1016/j.jtos.2020.03.006.

[5] A. Gordon-Shaag, M. Millodot, E. Shneor, The epidemiology and etiology of keratoconus, Int. J. Keratoconus Ectatic Corneal Dis. 1 (2012) 7–15, http://dx.doi.org/10.5005/jp-journals-10025-1002.

[6] S. Akhtar, A.J. Bron, S.M. Salvi, N.R. Hawksworth, S.J. Tuft, K.M. Meek, Ultrastructural analysis of collagen fibrils and proteoglycans in keratoconus, Acta Ophthalmol. 86 (2008) 764–772, http://dx.doi.org/10.1111/j.1755-3768.2007.01142.x.

[7] W.M. Petroll, M. Miron-Mendoza, Mechanical interactions and crosstalk between corneal keratocytes and the extracellular matrix, Exp. Eye Res. 133 (2015) 49–57, http://dx.doi.org/10.1016/j.exer.2014.09.003.

[8] A. Martínez-Abad, D.P. Piñero, New perspectives on the detection and progression of keratoconus, J. Cataract. Refract. Surg. 43 (2017) 1213–1227, http://dx.doi.org/10.1016/j.jcrs.2017.07.021.

[9] A. Pandolfi, F. Manganiello, A model for the human cornea: Constitutive formulation and numerical analysis, Biomech. Model. Mechanobiol. 5 (2006) 237–246, http://dx.doi.org/10.1007/s10237-005-0014-x.

[10] A. Gefen, R. Shalom, D. Elad, Y. Mandel, Biomechanical analysis of the keratoconic cornea, J. Mech. Behav. Biomed. Mater. 2 (2009) 224–236, http://dx.doi.org/10.1016/j.jmbbm.2008.07.002.

[11] A.S. Roy, W.J. Dupps, Patient-specific computational modeling of keratoconus progression and differential responses to collagen cross-linking, Invest. Ophthalmol. Vis. Sci. 52 (2011) 9174–9187, http://dx.doi.org/10.1167/iovs.11-7395.

[12] A.S. Roy, K.M. Rocha, J.B. Randleman, R.D. Stulting, W.J. Dupps, Inverse computational analysis of invivo corneal elastic modulus change after collagen crosslinking for keratoconus, Exp. Eye Res. 113 (2013) 92–104, http://dx.doi.org/10.1016/j.exer.2013.04.010.

[13] B.W.J. Dupps, I. Seven, A large-scale computational analysis of corneal structural response and ectasia risk in myopic laser refractive surgery (an american ophthalmological society thesis), Trans. Am. Ophthalmol. Soc. 114 (2016) 1.

[14] A. Pandolfi, A. Gizzi, M. Vasta, A microstructural model of cross-link interaction between collagen fibrils in the human cornea, Phil. Trans. R. Soc. A 377 (2019) http://dx.doi.org/10.1098/rsta.2018.0079.

[15] A. Gizzi, M.L.D. Bellis, M. Vasta, A. Pandolfi, Diffusion-based degeneration of the collagen reinforcement in the pathologic human cornea, J. Engrg. Math. 127 (2021) 1–10, http://dx.doi.org/10.1007/s10665-020-10088-x, 10.1007/s10665-020-10088-x.

[16] A. Alkanaan, R. Barsotti, O. Kirat, T. Almubrad, A. Khan, S. Akhtar, Ultrastructural study of peripheral and central stroma of keratoconus cornea, British Journal of Ophthalmology 101 (2017) 845–850, http://dx.doi.org/10.1136/bjophthalmol-2016-309834.

[17] C. Giraudet, J. Diaz, P.L. Tallec, J.M. Allain, Multiscale mechanical model based on patient-specific geometry: Application to early keratoconus development, J. Mech. Behav. Biomed. Mater. 129 (2022) http://dx.doi.org/10.1007/s10665-020-10088-x.

[18] I. Simonini, A.N. Annaidh, A. Pandolfi, Numerical estimation of stress and refractive power maps in healthy and keratoconus eyes, J. Mech. Behav. Biomed. Mater. 131 (2022) 105252, http://dx.doi.org/10.1016/j.jmbbm.2022.105252, https://linkinghub.elsevier.com/retrieve/pii/S1751616122001667.

[19] N. Falgayrettes, E. Patoor, F. Cleymand, Y. Zevering, J.M. Perone, Biomechanics of keratoconus: Two numerical studies, PLoS ONE 18 (2023) http://dx.doi.org/10.1371/journal.pone.0278455.

[20] E. Kuhl, A. Menzel, P. Steinmann, Computational modeling of growth. a critical review, a classification of concepts and two new consistent approaches, Comput. Mech. 32 (2003) 71–88, http://dx.doi.org/10.1007/s00466-003-0463-y.

[21] G. Himpel, Computational Modeling of Biomechanical Phenomena - Remodeling, Growth and Reorientation (Ph.D. thesis), Technical University of Kaiserslautern, 2007.

[22] S. Baek, J.D. Humphrey, Computational modeling of growth and remodeling in biological soft tissues: Application to arterial mechanics, Comput. Model. Biomech. (2010) 253–274, http://dx.doi.org/10.1007/978-90-481-3575-2_8.

[23] M.K. Rausch, A. Dam, S. Göktepe, O.J. Abilez, E. Kuhl, Computational modeling of growth: Systemic and pulmonary hypertension in the heart, Biomech. Model. Mechanobiol. 10 (2011) 799–811, http://dx.doi.org/10.1007/s10237-010-0275-x.

[24] C.J. Cyron, J.D. Humphrey, Growth and remodeling of load-bearing biological soft tissues, Meccanica 52 (2017) 645–664, http://dx.doi.org/10.1007/s11012-016-0472-5.

[25] J.D. Humphrey, Constrained mixture models of soft tissue growth and remodeling – twenty years after, J. Elasticity 145 (2021) 49–75, http://dx.doi.org/10.1007/s10659-020-09809-1.

[26] D. Guan, X. Zhuan, X. Luo, H. Gao, An updated lagrangian constrained mixture model of pathological cardiac growth and remodelling, Acta Biomater. 166 (2023) 375–399, http://dx.doi.org/10.1016/j.actbio.2023.05.022.

[27] D. Sachs, R. Jakob, B. Thumm, M. Bajka, A.E. Ehret, E. Mazza, Sustained physiological stretch induces abdominal skin growth in pregnancy, Ann. Biomed. Eng. (2024) http://dx.doi.org/10.1007/s10439-024-03472-6.

[28] D. Ambrosi, M.B. Amar, C.J. Cyron, A. DeSimone, A. Goriely, J.D. Humphrey, E. Kuhl, Growth and remodelling of living tissues: Perspectives, challenges and opportunities, J. Royal Soc. Interface 16 (2019) http://dx.doi.org/10.1098/rsif.2019.0233.

[29] G.A. Holzapfel, Nonlinear Solid Mechanics : A Continuum Approach for Engineering, Wiley, 2000.

[30] E.K. Rodriguez, A. Hoger, A.D. Mcculloch, Stress-dependent finite growth in soft elastic tissues, J. Biomch. 21 (1994) 455–467.

[31] A. Pandolfi, G. Fotia, F. Manganiello, Finite element simulations of laser refractive corneal surgery, Eng. Comput. 25 (2009) 15–24, http://dx.doi.org/10.1007/s00366-008-0102-5.

[32] P. Sánchez, K. Moutsouris, A. Pandolfi, Biomechanical and optical behavior of human corneas before and after photorefractive keratectomy, J. Cataract. Refract. Surg. 40 (2014) 905–917, http://dx.doi.org/10.1016/j.jcrs.2014.03.020.

[33] I. Simonini, A. Pandolfi, Customized finite element modelling of the human cornea, PLoS ONE 10 (2015) 1–23, http://dx.doi.org/10.1371/journal.pone.0130426.

[34] A. Pandolfi, G.A. Holzapfel, Three-dimensional modeling and computational analysis of the human cornea considering distributed collagen fibril orientations, J. Biomech. Eng. 130 (2008) http://dx.doi.org/10.1115/1.2982251.

[35] S. Wang, H. Hatami-Marbini, Constitutive modeling of corneal tissue: Influence of three-dimensional collagen fiber microstructure, J. Biomech. Eng. 143 (2021) http://dx.doi.org/10.1115/1.4048401.

[36] K.M. Meek, C. Boote, The use of x-ray scattering techniques to quantify the orientation and distribution of collagen in the corneal stroma, Prog. Retin. Eye Res. 28 (2009) 369–392, http://dx.doi.org/10.1016/j.preteyeres.2009.06.005.

[37] J.B. Randleman, D.G. Dawson, H.E. Grossniklaus, B.E. McCarey, H.F. Edelhauser, Depth-dependent cohesive tensile strength in human donor corneas: Implications for refractive surgery, J. Refract. Surg. 24 (2008) http://dx.doi.org/10.3928/1081597x-20080101-15.

[38] D.Z. Reinstein, T.J. Archer, J.B. Randleman, Mathematical model to compare the relative tensile strength of the cornea after prk asik, and small incision lenticule extraction, J. Refract. Surg. 29 (2013) 454–460, http://dx.doi.org/10.3928/1081597X-20130617-03.

[39] J.M. Dias, N.M. Ziebarth, Anterior and posterior corneal stroma elasticity assessed using nanoindentation, Exp. Eye Res. 115 (2013) 41–46, http://dx.doi.org/10.1016/j.exer.2013.06.004.

[40] K. Anderson, A. El-Sheikh, T. Newson, Application of structural analysis to the mechanical behaviour of the cornea, J. R. Soc. Interface 1 (2004) 3–15, http://dx.doi.org/10.1098/rsif.2004.0002.

[41] B. Fantaci, B. Calvo, R. Barraquer, A. Picó, M. Ángel Ariza-Gracia, Establishing standardization guidelines for finite-element optomechanical simulations of refractive laser surgeries: An application to photorefractive keratectomy, Transl. Vis. Sci. Technol. 13 (2024) 11, http://dx.doi.org/10.1167/tvst.13.5.11.

[42] Y.X. Wang, L. Xu, W.B. Wei, J.B. Jonas, Intraocular pressure and its normal range adjusted for ocular and systemic parameters. the beijing eye study, PLoS ONE 13 (2011) http://dx.doi.org/10.1371/journal.pone.0196926.

[43] M. Ariza-Gracia, J. Zurita, D.P. Piñero, B. Calvo, J.F. Rodríguez-Matas, Automatized patient-specific methodology for numerical determination of biomechanical corneal response, Ann. Biomed. Eng. 44 (2016) 1753–1772, http://dx.doi.org/10.1007/s10439-015-1426-0.

[44] T.T. Andreassen, A.H. Simonsen, H. Oxlund, Biomechanical properties of keratoconus and normal corneas, Exp. Eye Res. 31 (1980) 435–441.

[45] A. Eliasy, A. Abass, B.T. Lopes, R. Vinciguerra, H. Zhang, P. Vinciguerra, R. Ambrósio, C.J. Roberts, A. Elsheikh, Characterization of cone size and centre in keratoconic corneas, J. R. Soc. Interface 17 (2020) http://dx.doi.org/10.1098/rsif.2020.0271.

[46] M.W. Belin, G. Kundu, N. Shetty, K. Gupta, R. Mullick, P. Thakur, Abcd: A new classification for keratoconus, Indian J. Ophthalmol. 68 (2020) 2831–2834, http://dx.doi.org/10.4103/ijo.IJO_2078_20.

[47] T. Doll, J. Moore, A.H. Shihab, B.T. Lopes, A. Eliasy, O. Maklad, R. Wu, L. White, S. Jones, A. Elsheikh, A. Abass, Which feature influences on-eye power change of soft toric contact lenses: Design or corneal shape? PLoS ONE 15 (2020) http://dx.doi.org/10.1371/journal.pone.0242243.

[48] S. Kwok, N. Hazen, K. Clayson, X. Pan, J. Liu, Regional variation of corneal stromal deformation measured by high-frequency ultrasound elastography, Exp. Biol. Med. 246 (2021) 2184–2191, http://dx.doi.org/10.1177/15353702211029283.

[49] S. Yang, J. Zhang, Y. Tan, Y. Wang, Unraveling the mechanobiology of cornea: From bench side to the clinic, Front. Bioeng. Biotechnol. 10 (2022) http://dx.doi.org/10.3389/fbioe.2022.953590.

[50] M.C. Kenney, D.J. Brown, The cascade hypothesis of keratoconus, Contact Lens and Anterior Eye 26 (3) (2003) 139–146, http://dx.doi.org/10.1016/S1367-0484(03)00022-5.